

Engineering indefinitely long-lived localization in cavity-QED arrays

Amit Dey and Manas Kulkarni

International Centre for Theoretical Sciences, Tata Institute of Fundamental Research, Bengaluru – 560089, India

(Received 19 September 2019; revised manuscript received 3 March 2020; accepted 3 March 2020; published 1 April 2020)

By exploiting the nonlinear nature of the Jaynes Cumming interaction, one can get photon population trapping in cavity-QED arrays. However, the unavoidable dissipative effects in a realistic system would destroy the self-trapped state by continuous photon leakage, and the self-trapping remains only as a temporary effect. To circumvent this issue, we aim to achieve an indefinitely long-lived *self-trapped steady state* rather than a localization with limited lifetime. We show that a careful engineering of drive, dissipation, and Hamiltonian results in achieving indefinitely sustained self-trapping. We show that the intricate interplay between drive, dissipation, and light-matter interaction results in requiring an optimal window of drive strengths in order to achieve such nontrivial steady states. We treat the two-cavity and four-cavity cases by using exact open quantum many-body calculations. Additionally, in the semiclassical limit we scale up the system to a long one-dimensional chain and demonstrate localized and delocalized steady-states in a driven-dissipative cavity-QED lattice. Although our analysis is performed by keeping cavity-QED systems in mind, our work is applicable to other driven-dissipative systems where nonlinearity plays a pivotal role.

DOI: [10.1103/PhysRevA.101.043801](https://doi.org/10.1103/PhysRevA.101.043801)**I. INTRODUCTION**

Intricate interplay between the nonlinear interactions and kinetic hopping delivers fascinating physics of Josephson oscillation and macroscopic quantum self-trapping, which are already realized in bosonic Josephson junctions (BJJs) consisting of cold-atomic Bose-Einstein condensates (BECs) [1–4]. The novel phenomenon of self-trapping is a consequence of strong nonlinear on-site interaction that dominates the particle tunneling. Despite short-lived polariton states and weak photon-photon interaction [5–7], nonlinear Josephson oscillation as well as macroscopic self-trapping have been achieved in photonic systems (e.g., cavity-QEDs, see Fig. 1) characterized by light-matter interactions [8–12].

Photonic Josephson junctions (PJJs) have come up as a novel platform for quantum many-body simulation [11]. An extended version of PJJs can be realized in a lattice of cavities with nearest-neighbor tunneling. Realizations of large bosonic systems, such as a Bose-Hubbard lattice [13–15] of ultracold atoms and strong light-matter coupling [16] have motivated exploration of strongly correlated phases in cavity-QED arrays. Scaled-up cavity arrays with various coordination numbers can offer exotic collective many-body phenomena often missed in few-body physics (e.g., Mott insulator). In these setups, the Mott insulator to superfluid phase transition is investigated [17–20]. Addressing dissipation engineering in a cavity network, a purely-dissipation-induced phase transition from a superfluid-like state to a Mott-insulator-like state was predicted beyond a critical cavity decay [10,21]. Additionally, drawing correspondence to Bose-Hubbard dynamics, driven-dissipative cavity arrays are presented as efficient quantum simulators [22,23] implementable with present technology. Moreover, a dissipative phase transition has been observed experimentally in a one-dimensional (1-D) lattice of

72 microwave cavities, each coupled to a superconducting qubit [24]. Thus, substantial progress has been made regarding scalable cavity-QED based architectures [25]. Given these experimental and theoretical advances in large-scale systems, exploring the possibility of nontrivial nonequilibrium steady states is an interesting avenue of research.

Dissipation-induced delocalization-localization transitions of photons were theoretically predicted [11] and experimentally verified [12]. The critical atom-photon interaction for such a transition is large and can be well achieved in a cavity consisting of superconducting qubits coupled to transmission line resonators [26,27]. Although self-trapping is achieved in a coupled cavity dimer, continuous unavoidable photon leakage and spontaneous decay of the qubit limit the longevity of self-trapped states in a realistic system [11]. Therefore, it is imperative that competition of dissipation, drive, and interaction strength be explored in detail and requirements for robust localization are sought. In fact, the idea of striking a delicate balance between drive and dissipation has been very successful in preparing target states [28], achieving indefinitely long-lived entanglement between qubits [29–32] and persistent chiral currents [33].

Here, we investigate a strong-coupling regime where both drive and dissipation are present and hope to create photon-localized steady states. For smaller systems, we do a brute-force open quantum many-body treatment involving the standard quantum master-equation approach to a density matrix and a quantum Monte Carlo wave-function method [34] for a slightly bigger system. In the semiclassical limit, we investigate a long 1-D driven-dissipative lattice model. Our key findings can be categorized as follows: (i) There exists an optimal window of drive strength where a localized steady state is obtained. As a consequence of this, we get interesting phase diagrams. (ii) For a closed system with

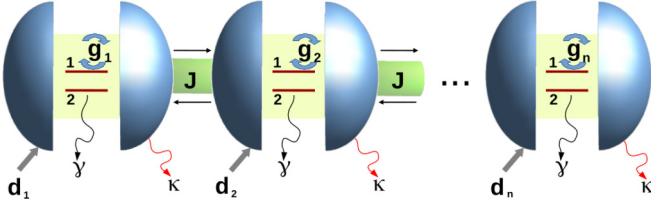


FIG. 1. Schematic depiction of 1-D lattice of identical cavity-QEDs, each containing a two-level system with levels marked 1 and 2. Each two-level system is coupled to the cavity photons with a strength g_i . Additionally, J , κ , γ represent intercavity tunneling, photon decay, and spontaneous decay of the two-level system, respectively. d_i is the coherent photon microwave drive applied at the i th cavity.

subcritical light-matter interactions, there is no localization effect. On the contrary, by incorporating drive and dissipation into the system it is possible to achieve a *self-trapped steady state* at the same light-matter coupling strengths. (iii) The achieved self-trapped steady state is independent of the initial-state preparation which is immensely beneficial, especially from an experimental perspective. Furthermore, preparation independence of our exotic steady states clearly states that long-time localization does not care whether the light-matter interaction is critical or subcritical with respect to the initial photon population. This feature reflects the clear distinction between our *self-trapped steady states* and temporary localization achieved previously [11,12]. Specifically, we attempt a dissipative preparation of novel self-trapped states and analyze how this protocol depends on the parameter space.

II. MODEL AND APPROACHES

The Hamiltonian defined for cavity-QED arrays in a rotating frame of drive frequency (ω_p) is given by

$$H = \sum_i H_i - J \sum_{(ij)} (a_i^\dagger a_j + \text{H.c.}), \quad (1)$$

where $H_i = (\omega_0 - \omega_p) s_i^z + (\omega_c - \omega_p) a_i^\dagger a_i + g_i (a_i^\dagger s_i^- + a_i s_i^+) + d_i (a_i + a_i^\dagger)$. Here, ω_0 and ω_c are the characteristic frequencies of the qubit (embedded in the cavity) and cavity photons, respectively; a_i destroys photon at the i th cavity, and s_i^α (where $\alpha \equiv \{x, y, z\}$) is the i th qubit. g_i is the qubit-photon coupling strength that dictates the Rabi oscillations of excitation dynamics and d_i is the drive strength. As per the experimental scenario, we introduce the qubit (spontaneous) decay rate γ and the photon leakage κ of the cavity. Such considerations forces us to treat this as an open system whose zero-temperature dynamics could be described by the Lindblad master equation written as $\dot{\rho}(t) = -i[H, \rho(t)] + \kappa \sum_j \mathcal{L}[a_j] + \gamma \sum_j \mathcal{L}[s_j^-]$ where $\mathcal{L}[A_j] = [2A_j \rho(t) A_j^\dagger - A_j^\dagger A_j \rho(t) - \rho(t) A_j^\dagger A_j]/2$ takes account the dissipation involved with the qubit or photonic degrees of freedom. $\rho(t)$ is the reduced density matrix of the system. Here we mainly focus on low-temperature behavior where the thermal photon contribution is neglected and only coherent photon drive is employed. Furthermore, we calculate the average photon number and average spin as $N_i =$

$\text{Tr}[a_i^\dagger a_i \rho(t)]$ and $\langle s_i^\alpha \rangle = \text{Tr}[s_i^\alpha \rho(t)]$, respectively. We solve the above Lindblad master equation by two approaches: (i) The traditional numerical implementation of the above equation and (ii) a quantum Monte Carlo wave-function method, which is a powerful technique to deal with a larger Fock space [34].

It is also imperative to mention an important experimentally feasible limit. In the large-photon-number limit [11] one can efficiently approximate the second-order correlation with the product of first-order expectation values. In other words, $\langle a_i s_i^+ \rangle \approx \langle a_i \rangle \langle s_i^+ \rangle$ and so on. Using the above Lindblad equation and exploiting the semiclassical approximation, we get

$$\begin{aligned} \langle \dot{a}_j(t) \rangle = & -i(\omega_c - \omega_p) \langle a_j(t) \rangle - ig_j \langle s_j^-(t) \rangle \\ & + iJ[\langle a_{j+1}(t) \rangle + \langle a_{j-1}(t) \rangle] - \frac{\kappa}{2} \langle a_j(t) \rangle - id_j, \end{aligned} \quad (2)$$

$$\begin{aligned} \langle \dot{s}_j^-(t) \rangle = & -i(\omega_0 - \omega_p) \langle s_j^-(t) \rangle + 2ig_j \langle a_j(t) \rangle \langle s_j^z(t) \rangle \\ & - \frac{\gamma}{2} \langle s_j^-(t) \rangle, \end{aligned} \quad (3)$$

$$\begin{aligned} \langle \dot{s}_j^z(t) \rangle = & -ig_j [\langle s_j^+(t) \rangle \langle a_j(t) \rangle - \langle a_j^+(t) \rangle \langle s_j^-(t) \rangle] \\ & - \gamma \left[\langle s_j^z(t) \rangle + \frac{1}{2} \right]. \end{aligned} \quad (4)$$

In the semiclassical limit the expectation values of the operators can be expressed as complex numbers. To investigate the population-trapping phenomenon we rely on the population imbalance

$$z(t) = \frac{\sum_{i=1}^M (-1)^{i+1} N_i}{\sum_{i=1}^M N_i},$$

where $N_i = |\langle a_i \rangle|^2$. We designate the state of the system as $\{N_i, \langle s_i^z \rangle\}$. For $M = 2$, we start with the configuration $\{N, 0, -1/2, -1/2\}$ and analyze the steady-state values of z with varying g_i , d_i , κ , and γ . Using canonical transformation, it has been perturbatively shown that the Jaynes-Cummings interaction induces on-site photon-photon coupling that provides a nonlinear contribution to the bare photon dynamics [35]. This perturbative regime (dispersive case) is, however, not our subject of focus here. For the resonant case, the effective anharmonicity is expected to be the strongest. In such a resonant situation we analyze the role of dissipation, drive, and nonlinear interaction together and present the results in next section.

III. RESULTS

In this section, we present results for both (i) the fully quantum case and (ii) the semiclassical limit. Throughout the paper we stick to the near-resonant case $\omega_0 - \omega_p = \omega_c - \omega_p = 0.01J$. It is important to note that we express the light-matter interaction in terms of critical coupling g_c [11] only when we present results for a fully closed-system (with no dissipation and drive, i.e., an isolated quantum system). On the other hand, a driven-dissipative system has no connection with g_c .

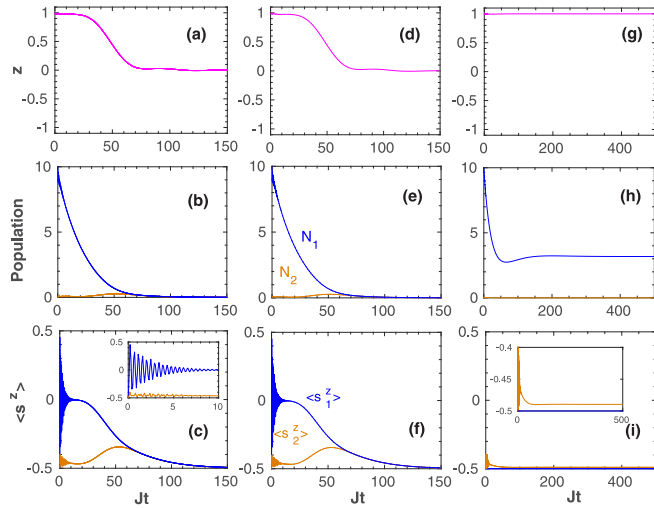


FIG. 2. Quantum dynamics for two coupled cavities are presented for initial state $\{10, 0, -1/2, -1/2\}$ and $\kappa = \gamma = 0.04J$. Panels (a)–(c) are undriven cases when $g_1 = g_2 = 17.7J$. Panels (d)–(f) are drawn for $d_1 = 0.04J$, $d_2 = 0$, and $g_1 = g_2 = 17.7J$, i.e., light-matter coupling in both cavities are turned on. Panels (g)–(i) are cases when $g_1 = 0$, $g_2 = 17.7J$, and the driving intensities are the same as in panel (d). N_i and s_i^z are mentioned with similar colors as the respective lines. This demonstrates that indefinite self-trapping can be achieved when one of the cavities does not have light-matter coupling.

A. Results from quantum simulation

Here we carry on full quantum treatment for a case with relatively small number of photons and solve the Lindblad master equation in a many-body framework. The undriven case in Figs. 2(a)–2(c) shows that dissipation limits the lifetime of localization (as will be seen even in the semiclassical picture in a subsequent discussion). Comparing Figs. 2(b) and 2(c) we see that the qubit energy in the second cavity increases whenever the photon population N_2 shows a bump in Fig. 2(b). The inset of Fig. 2(c) also addresses rapid decay of Rabi oscillations. In Figs. 2(d)–2(f) we coherently drive the first cavity but no enhancement of localization is observed. In fact, we find (not shown here) only a small enhancement even when much larger driving intensities (such that $g_1, g_2 \neq 0$) are considered. This behavior makes the quantum scenario strikingly different from the semiclassical case (as will be discussed in the next section) where quantum correlation is ignored. Such a purely quantum effect restricts the external photons making the drive ineffective and thereby making the localized steady state unattainable (until we go to extremely high drives which is computationally challenging).

The dynamics of photon-photon correlation in terms of the $g^{(2)}$ function is presented in Fig. 3, where we plot temporal behavior of undelayed second-order correlation, given by $g^{(2)}(\tau)|_{\tau=0} = \langle a_1^\dagger(t+\tau)a_1^\dagger(t)a_1(t+\tau)a_1(t) \rangle / \langle a_1^\dagger(t)a_1(t) \rangle^2|_{\tau=0}$ (of first cavity). Figure 3(a) shows that an antibunching-to-bunching transition occurs earlier when the cavity-qubit coupling is switched off for the first cavity. On the other hand, when light-matter interaction $g \neq 0$ for both the cavities, this transition appears at a time where the blockade in the right cavity is already broken and the

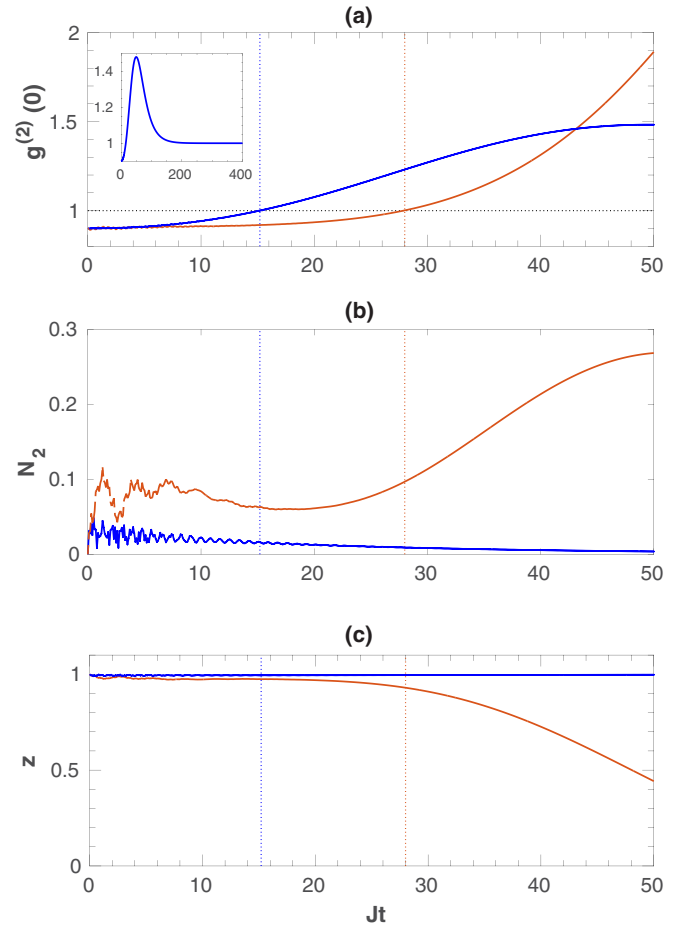


FIG. 3. (a) Dynamics of quantum correlation function $g^{(2)}(0)$. The horizontal dotted black line in panel (a) marks the $g^{(2)}(0) = 1$ value. (b) N_2 dynamics. (c) Short-time dynamics of z is shown for the two cases. Vertical dotted lines of respective colors mark the times when $g^{(2)}(0)$ attains 1 in all figures. Parameter values are same as in Fig. 2(d) [solid orange (gray), $g_1 = g_2$] and Fig. 2(g) [solid blue (dark), $g_1 = 0, g_2 \neq 0$], respectively.

localization starts getting lost [see Figs. 3(b) and 3(c)]. Furthermore, the inset in Fig. 3(a) describes coherent light at long times for the former case. This is obvious because the steady state describes an empty second cavity and a first cavity with only noninteracting photons [see Fig. 2(h)]. We thus demonstrate that antibunching in the first cavity (which is also the driven) is enhanced when $g_1 \neq 0$ which thereby disallows self-trapping. We nullify this correlation by switching off the cavity-qubit coupling only in the first cavity (i.e., making $g_1 = 0$) and plot the results in Figs. 2(g)–2(i). Figure 2(g) presents a localized steady state at the same d_1 value as in Fig. 2(d); Fig. 2(h) supports the attainment of finite steady-state population for the first cavity and a vacuum for the second cavity. Figure 2(i) shows that the isolated first qubit remains in its ground state, whereas the second qubit shows some dynamics because $g_2 \neq 0$ [see inset of Fig. 2(i)]. Therefore, we have demonstrated that, by carefully engineering the Hamiltonian, one can achieve an indefinitely long-lived self-trapped steady state in a fully quantum system. The question if the nonuniform light-matter coupling ($g_1 \neq g_2$) is a necessary

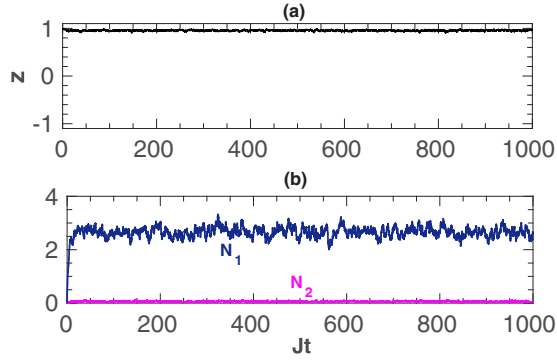


FIG. 4. Full quantum treatment of a two-cavity case with uniform couplings. Attainment of self-trapped steady state is established when $g_1 = g_2 = 10J$, $\kappa = \gamma = 1.6J$, $d_1 = 4J$, and $d_2 = 0$. The N_i are mentioned with similar colors as the respective lines.

condition in achieving long-lived self trapping may arise here. Figure 4 establishes that a quantum case with strong uniform coupling will also produce a self-trapped steady state. Here we use a very strong drive (to dodge strong antibunching in cavity 1) along with strong dissipation to tackle Hilbert-space size when achieving numerical convergence. A nonuniform coupling is not a necessary condition but it seems to be a good strategy to trap a larger number of photons using a much weaker drive.

We scale up the quantum case to a 1-D chain of four cavity-QEDs and plot the results in Fig. 5 when only the first and third cavities are initially populated. With finite γ and κ , z decays in Fig. 5(a) (light blue). On the other hand, the driven-dissipative situation (thick black) localizes the photon populations in the first and third cavities [see Figs. 5(b)–5(e)]. This figure demonstrates the steady-state localization in an extended open quantum system. Here we used small values for d_i so that the Hilbert-space size of the four-cavity case can be tackled numerically. For larger drive strengths we will need larger Fock-space cutoff in the numerics to take into account the presence of large numbers of photons.

Figure 6 demonstrates the initial-state independence of the steady states achievable in this open quantum system. In addition to this being interesting, it is also more practical from an experimental perspective to start with a vacuum state in the cavities and $s_i^z = -1/2$ for the qubits. Additionally, the degree of nonlinearity having no dependence on the initial photon number makes our steady-state localization markedly different from the delocalization-localization transition in Ref. [11]. Such a setup when driven out of equilibrium leads to interesting nonequilibrium steady states, which in our case is dictated only by γ , κ , d_i , and g_i . A more elaborate description of initial-state independence for widely varying initial states is presented in Fig. 10 of Appendix A. In Figs. 6(a)–6(c) we find that an optimum drive $d_1 = 0.04J$ produces a self-trapped steady state, whereas an over-drive $d_1 = 0.2J$ populates the undriven second cavity, destroying strong self-trapping [see Fig. 6(c)] and leading only to a partially self-trapped state. Next, we present the semiclassical results for a long 1-D chain, when comparatively large numbers of photons are considered.

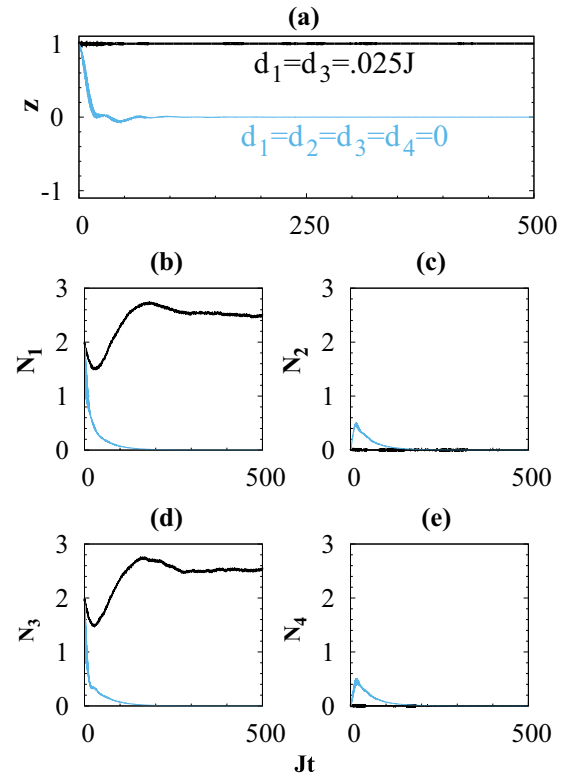


FIG. 5. Quantum dynamics for a 1-D chain of four cavities, when the initial conditions are $\{2, 0, 2, 0\}$ for the cavity photon population and $\{-1/2, -1/2, -1/2, -1/2\}$ for the qubits. The results are nonetheless independent of initial conditions as shown in Fig. 6 (and in Appendix A). (a) Dynamics of z is presented for $\gamma = \kappa = .02J$, $M = 4$, $g_2 = g_4 = 17.8J$, and $g_1 = g_3 = 0$. The undriven case having $d_i = 0$ (thin light blue) is contrasted with a case where $d_1 = d_3 = .025J$ and $d_2 = d_4 = 0$ (thick black). Panels (b)–(e) describe the photon population of four cavities.

B. Semiclassical results

In a semiclassical framework we neglect the quantum correlations and make use of Eqs. (2)–(4). We present results for a 1-D lattice of identical cavities. We investigate $M = 100$ cavities each hosting a qubit with identical couplings $g_i = g$. Although we can tackle much larger lattices, the essential physics remains the same. Without loss of generality, we choose initial conditions such that all the odd cavities are populated and all the even cavities are vacant. The defined population imbalance z is plotted in Figs. 7(a) and 7(b). The closed-system case is shown in Fig. 7(a) which shows localization when $g \approx 2g_c$ with $g_c = 2.8\sqrt{N}J$ (where N is the initial photon number on every odd site) [11]. In contrast with the two-cavity closed-system case ($M = 2$) in Fig. 11(d), here we need $g = 2g_c$ for localization. The factor of two is essentially the coordination number. Here one should note that the critical coupling g_c has relevance to the closed-system case only and does not relate to our driven-dissipative steady-state localization. We present this particular case only for comparison. In Fig. 7(b) the driven-dissipative scenario is presented where appropriately driven odd sites stabilize the localized state. These results indicate that drive and dissipation can be carefully designed to create localized

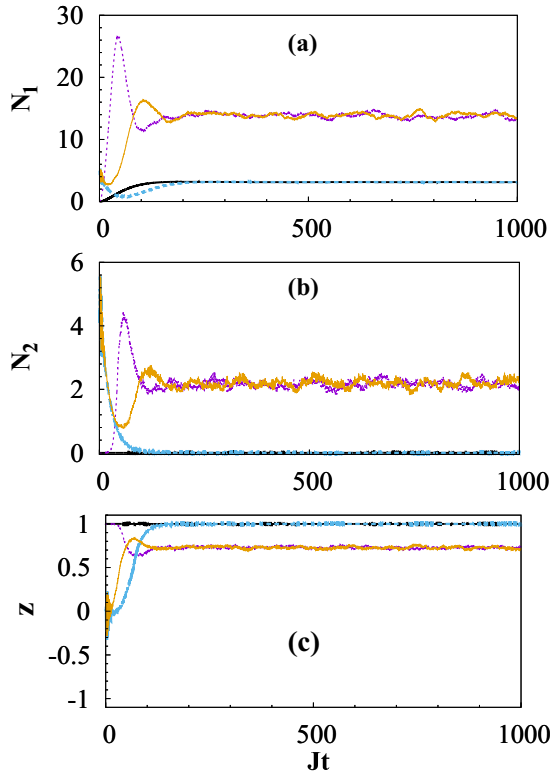


FIG. 6. Quantum dynamics and demonstration of initial-condition independence. Here $M = 2$, $\gamma = \kappa = 0.04J$, and $g_1 = 0$, $g_2 = 10.62J$. Plots are shown for two distinct initial conditions: (i) $N_1 = N_2 = 0$ (both cavities are initially vacuum presented by solid black and dotted purple) and (ii) $N_1 = N_2 = 5$ [presented by dashed blue and solid yellow (thin gray)]. For each initial condition we show results for two $\{d_1, d_2\}$ compositions: (i) $d_1 = 0.04J$, $d_2 = 0$ (black and dashed blue) and (ii) $d_1 = 0.2J$, $d_2 = 0$ [dotted purple and solid yellow (thin gray)]. Panels (a)–(c) plot N_1 , N_2 , and z dynamics, respectively. The initial-condition independence can be seen in our results. The initial conditions for qubits in all cases were $\{-1/2, -1/2\}$ but we find that the initial-condition independence also holds for different initial conditions of the qubits (see Fig. 10 in Appendix A).

steady states in large-scale systems. At t_{break} (where the self trapping is just disrupted) rapid oscillation of z sets in and this indicates photon tunneling throughout the lattice. We show only a few oscillations after t_{break} that converge for various numerical precisions. As we advance in time, subsequent oscillations become too sensitive to precision and barely give any relevant physical insight. This regime is anyway not of interest because the self-trapped phase is already destroyed and the photon populations at times $\gg t_{\text{break}}$ are too small to support the semiclassical approximation. A detailed analysis of these oscillations for a case of $M = 2$ is presented in Appendix B. Through our semiclassical analysis we also find that, as long as the system is in a self-trapped phase, the results are insensitive to the details of the initial state, thereby making it more experimentally feasible. The conditions for the semiclassical approximation to hold is in tune with the current experimental setups [12]. From the above diagram (Fig. 7), one can notice that an intricate interplay between

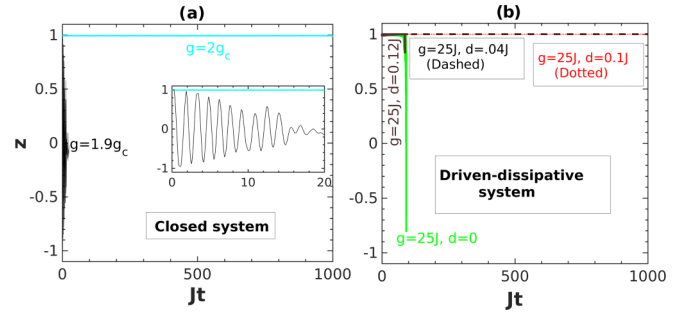


FIG. 7. Semiclassical dynamics for population imbalance in a 1-D lattice consisting 100 identical cavity-QEDs (each hosting a qubit) is presented with g_i and d_i values mentioned with similar colors as the respective lines. In all cases every odd cavity is initialized with 20 photons and even cavity is kept vacant. κ , γ , and $g_i = g$ values are kept identical for each cavity in the array. (a) Depiction of delocalization-localization transition for a closed-system case (no drive and dissipation). (b) Open-system case (i.e., with drive and dissipation) with $\kappa = \gamma = 0.04J$ which reflects stabilization (indefinitely long lived) of self-trapped state with appropriate drive. Here, $g_c = 2.8J\sqrt{20}$ is only defined for the closed-system case in panel (a).

drive, dissipation, and interaction can lead to the existence of an optimal window of drive strengths where localized steady states can exist. This naturally leads to an interesting question regarding the existence of a phase diagram in such systems. We investigate this for the case of $M = 2$ without loss of generality.

Figure 8 ($M = 2$) demonstrates an interesting phase diagram. In Fig. 8(a) we see that there is a minimum drive d_1^{min} and a maximum drive d_1^{max} for a given value of cavity decay κ (keeping all other parameters fixed) and they define

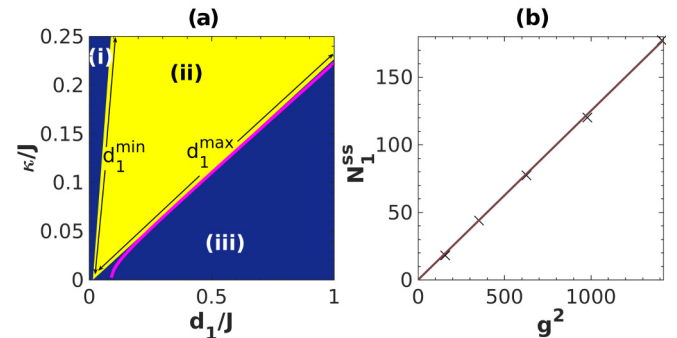


FIG. 8. (a) Semiclassically obtained phase-space description of long-lived self-trapped state in d_1 - κ plane, when $\gamma = 0.04J$. The cavity system is initialized to a state $\{20, 0, -1/2, -1/2\}$ and the coupling for both the cavities $g_1 = g_2 = g = 25J$. The three phases in this figure are (i) under-driven non-self-trapped, (ii) indefinitely self-trapped, and (iii) over-driven delocalized. The limiting values d_1^{min} and d_1^{max} lie on the lower and upper boundaries of phase (ii), respectively. The magenta line gives an analytical prediction for the curve $\kappa(d_1)$ representing the boundary between phases (ii) and (iii). (b) For various values of g , $d_1 = d_1^{\text{max}}$ is obtained for $\kappa = 0.1J$ and $\gamma = 0.04J$. N_1^{ss} is numerically found for these parameter values and plotted (by “ \times ” markers) with respect to g^2 . A solid line is plotted for $N_1^{\text{ss}} = (1/8)g^2$ that nicely fits the data points.

the limiting drives for steady-state localization. The minimum drive can be understood as the least amount of driving needed to assure reasonable population in the first cavity in comparison with the second one. The maximum drive suggests that the driving beyond a point leads to population increase in the other cavity, thereby destroying self-trapping. Depending upon the nature and lifetime of localization we divide the phase space into three regions: (i) under-driven non-self-trapped, (ii) indefinitely self-trapped, and (iii) over-driven delocalized regions. Phase (i) is dissipation dominated and photon numbers gradually become too small and the system enters the quantum regime. The semiclassical approximation does not hold in this regime and fails to predict if there exists a small steady-state population N_1 . However, the monotonic decay of population due to strong dissipation suggests that no considerable population is trapped in the first cavity at steady state. In fact, in this regime, even via fully quantum simulations, we demonstrate that this phase does not have self-trapping. Phase (ii) represents the system having self-trapping in its steady state. Here drive, dissipation, and light-matter coupling make a delicate balance. Phase (iii) deals with an over-driven situation. By over-drive we mean $d_1 > d_1^{\max}$ that limits the localization lifetime by populating the second cavity. In this case, N_1 is quite large around t_{break} , making the semiclassical treatment valid [see Fig. 13(c) of Appendix B]. After t_{break} , at least a few oscillations of large population are physically meaningful, describing the dynamical delocalization of an already localized state (having lifetime $0 < t < t_{\text{break}}$). Neither of the phases (i) and (iii) supports indefinite localization. N_1 monotonically decays in phase (i) without populating the second cavity and N_1, N_2 become comparable. On the contrary, in phase (iii) N_1 initially grows to a value and then starts oscillations by populating the second cavity. Therefore, d_1^{\max} demarcates two physically distinct phases of localization. For further details about different phases see discussions in Appendix B.

The upper limit of “good” drive d_1^{\max} can be analytically discussed. Assuming that there is steady-state self-trapping, one gets the relation: $\kappa(d_1) = 2[(\frac{d_1^2}{N_1^{ss}}) - (\omega_c - \omega_p)^2]^{1/2}$, where N_1^{ss} defines the steady-state population of the first cavity. The above equation is derived from Eqs. (2)–(4) with the assumption that the cavity 2 is effectively disconnected since $\langle a_2 \rangle \approx 0$. Moreover, we assume that the qubit in the first cavity plays no role because $\langle s_1^- \rangle \approx 0$. These assumptions can be supported by a brute force simulation. Having justified these assumptions via a brute force simulation, we find that the above analytical formula fits remarkably well with the numerical results. Now, the $\kappa(d_1)$ equation is defined for a particular value of g because the assumption of steady-state self trapping itself depends on the degree of light-matter interaction. Indeed, we find different slopes for the upper boundary d_1^{\max} for various g values. A natural question is to find the dependence of steady-state population N_1^{ss} on g . By choosing κ and d_1 values right on the upper boundary of localized steady-state region for various g values, we numerically extract N_1^{ss} and plot Fig. 8(b). By straight-line fitting we infer that a localized steady state for particular values of $\kappa, \gamma, d_1^{\max}$ obeys the relation $N_1^{ss} \approx (1/8)g^2$. Using this relation we can write the $\kappa(d_1)$ equation as $\kappa(d_1) = 2[8(\frac{d_1^2}{g^2}) - (\omega_0 - \omega_p)^2]^{1/2}$

which is given by the magenta line in Fig. 8(a). Indeed, we would like to point out again that, in the regime where the analytical curve agrees with the numerical phase boundary, the numerical results show that $\langle s_1^- \rangle$ and $\langle a_2 \rangle$ are negligible. For further analysis of the two-cavity case, see Figs. 11 and 12 in Appendix B. We would like to point out that we see a minor discrepancy between the analytical curve and the phase boundary from numerics [Fig. 8(a)] in the regime where κ is small. Now one may be interested in investigating γ dependence of the self-trapped region for a fixed κ . In Fig. 14(b) in Appendix B we see that d_1^{\max} remains almost fixed with increasing γ . This is a mere consequence of negligible photon loss via the spontaneous decay channel γ of the qubit (at a fixed κ).

One remarkable difference between the quantum and semiclassical treatments is the effectivity of d_1 . The strong antibunching of photons in Fig. 2(d) (with $g_1 \neq 0$) makes the cavity resistant to external drive. This effect is absent in semiclassics where we neglect the second-order correlation between the qubit and photons in the large- N limit.

Now we comment about the nature of localization in single and multiphoton regimes. The photon self-trapping in a multiphoton system stems from nonlinearity in the Hamiltonian. But it can also be achieved in a linear regime (where $N \approx 1$) by switching off the coupling in the first cavity ($g_1 = 0$). In this case, a $g_2 \gg J$ regime suppresses intercavity tunneling and effectively decouples the cavities. This feature is reflected even in a closed system, where $\{1, 0, -1/2, -1/2\}$ simply becomes an eigenstate in the limit $g_2 \gg J$ and remains stationary. When the system is made open, the first cavity attains some steady-state population without affecting the second cavity, provided that the photon injection rate in the first cavity remains small.

An important finding of our work is that, both in the quantum and semiclassical treatments, steady-state self-trapping can be attained for a driven-dissipative system with a certain light-matter interaction, whereas it is absent for a closed-system counterpart having the same interaction strength (implying a subcritical $g < g_c$ interaction for closed systems; see Fig. 9).

IV. DISCUSSION AND CONCLUSION

In this paper, we have studied an open system consisting of a 1-D lattice of cavities each hosting a qubit. This system is further subject to drive and dissipation. By striking a delicate balance between drive, dissipation, and interactions, we have predicted a parameter regime where an indefinitely-long-lived self-trapped state exists. Such exotic steady states are independent of initial-system preparation, which is advantageous for experiments. Our analysis of an engineered driven-dissipative cavity system will help in precisely accessing localization and delocalization phases and will also be paramount for well-controlled photon transport in a cavity array. It is worth noting that interesting studies regarding dissipative stabilization of nonequilibrium steady states in Bose-Hubbard lattices have been done with additional photon-photon Kerr nonlinearity [36–38].

Future outlook involves developing quantum methods for dealing with even larger systems. This could be key for

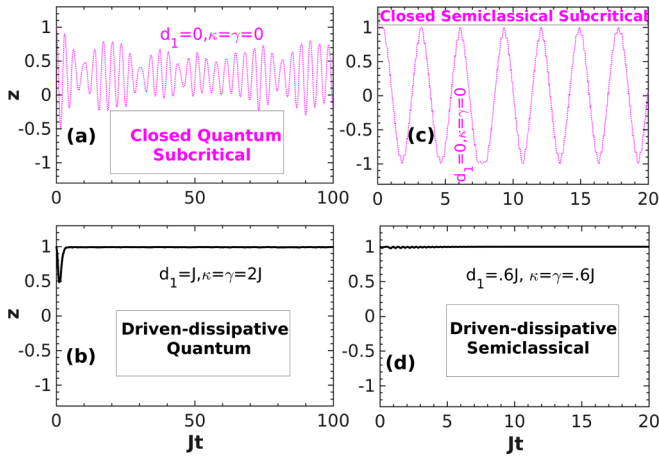


FIG. 9. Demonstration of driven-dissipative steady-state self-trapping for an interaction which is subcritical if considered for a closed-system counterpart. The two-cavity system is initialized at $\{20, 0, -1/2, -1/2\}$. Panels (a) and (b) describe quantum cases when $g_1 = 0$, $g_2 = 5J$. Panels (c) and (d) describe semiclassical cases when $g_1 = g_2 = 11.27J$. The critical interaction $g_c = 2.8\sqrt{20J}$ can only be defined for fully-closed-system cases in panel (a) $g_1 = 0$, $g_2 = 0.4g_c$ (expressed in terms of g_c) and panel (c) $g_1 = g_2 = 0.9g_c$. Drive and dissipation rates are mentioned for driven-dissipative cases in panels (b) and (d) with respective colors.

investigating indefinitely-long-lived many-body localization in driven-dissipative systems. The role of counter-rotating terms (e.g., Rabi-Hubbard) in the physics of self-trapping still remains unexplored. Needless to mention, the physics of localization remains fascinating in two or more dimensions and artificially engineered systems with deformable lattices [39].

ACKNOWLEDGMENTS

We would like to thank J. Keeling for useful discussions. M.K. gratefully acknowledges a Ramanujan Fellowship SB/S2/RJN-114/2016 from the Science and Engineering Research Board (SERB), Department of Science and Technology, Government of India. M.K. also acknowledges support from an Early Career Research Award, ECR/2018/002085 from the Science and Engineering Research Board (SERB), Department of Science and Technology, Government of India. M.K. would like to acknowledge support from the project 6004-1 of the Indo-French Centre for the Promotion of Advanced Research (IFCPAR).

APPENDIX A: INITIAL-STATE INDEPENDENCE OF STEADY STATE

Here we present full quantum result showing that the steady-state values are independent of the initial photon number distribution and qubit states. In Figs. 10(a)–10(c) various preparations approach unique steady states at long times. The final state is only dictated by κ , γ , d_1 , and the light-matter coupling.

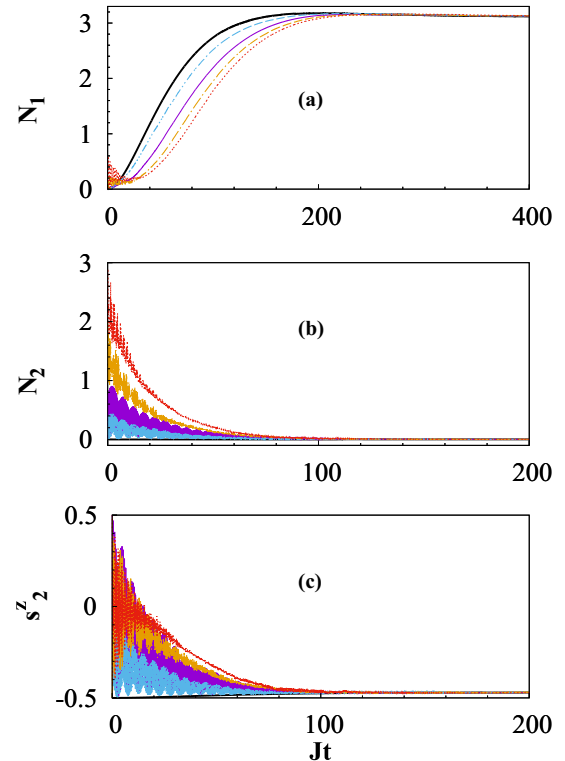


FIG. 10. Exact quantum simulation. Photon and qubit dynamics for various initial photon number distribution and qubit states. Here $\kappa = \gamma = 0.04J$, $d_1 = 0.04J$, $d_2 = 0$, and $g_1 = 0$, $g_2 = 10.63J$. Various preparations are as follows: (i) $\{0, 0, -1/2, -1/2\}$ (thick solid black), (ii) $\{0, 0, -1/2, 1/2\}$ (thin solid purple), (iii) $\{0, 0, -1/2, 0\}$, i.e., the qubit state in cavity 2 is an equal superposition of the excited and ground states (dashed blue), (iv) $\{0, 2, -1/2, -1/2\}$ (dashed dotted yellow), and (v) $\{0, 2, -1/2, 1/2\}$ (dotted red). At long time the uniqueness of the steady state is evident.

APPENDIX B: SEMICLASSICAL RESULTS FOR TWO COUPLED CAVITIES

In this Appendix we compare localization for various degrees of openness. We consider a two-cavity system with large number of photons and discuss the validity of our semiclassical approach. Furthermore, we pick up sets of parameters from phases (i)–(iii) and differentiate them by plotting the respective dynamics.

In Fig. 11 we plot dynamics of z for different couplings g , γ , κ , d_1 , and d_2 when only the first cavity is loaded with photonic population with initial state $\{20, 0, -1/2, -1/2\}$.

Figure 11(a) depicts the lossless coherent oscillation of undriven photonic population for $g = 0.9g_c$ whereas, in Fig. 11(b), the introduction of strong dissipation localizes z for a limited time and the population decays thereafter. The moment the localized state gets destroyed (marked by Jt_{break}), we get rapid oscillations due to decayed population. Figure 11(c) shows the dynamics of population distribution in the respective cavities. However, as dissipation reduces N_i , the modified critical condition suits the subcritical g and localization is established. A similar message is reflected in Figs. 11(d)–11(f) but for a case with coupling $g = 12.52J$ ($=g_c$ for a closed system). Comparing Figs. 11(d) and 11(e),

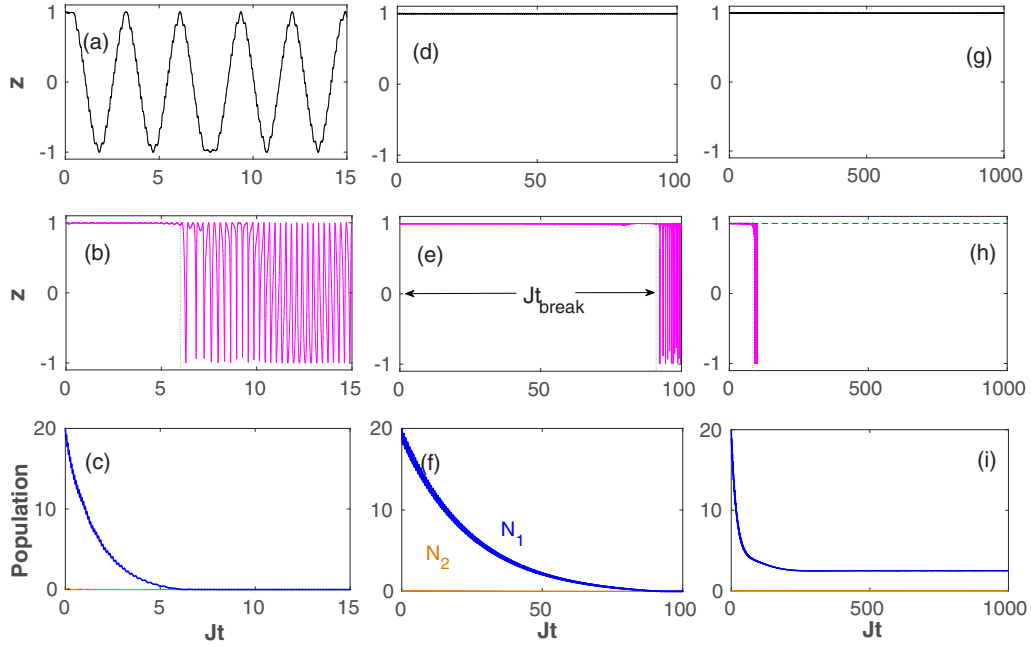


FIG. 11. Semiclassical behavior of population dynamics of two coupled cavities with varying γ , κ , $g_1 = g_2 = g$, and drive. Here, $g_c = 2.8J\sqrt{20}$ is defined for closed system. (a) $g = 0.9g_c$, $\gamma = 0$, $\kappa = 0$, and $d_1 = d_2 = 0$ (closed system with subcritical light-matter coupling). (b) $g = 11.27J$, $\gamma = 0.6J$, $\kappa = 0.6J$, and $d_1 = d_2 = 0$ (dissipative system with no drive). (d) $g = g_c$, $\gamma = 0$, $\kappa = 0$, and $d_1 = d_2 = 0$ (closed system with critical light-matter coupling). (e) $g = 12.52J$, $\gamma = 0.04J$, $\kappa = 0.04J$, and $d_1 = d_2 = 0$ (dissipative system with no drive). (g) $g = 2g_c$, $\gamma = 0$, $\kappa = 0$, and $d_1 = d_2 = 0$ (closed system with light-matter coupling greater than g_c). (h) $g = 25J$, $\gamma = 0.04J$, $\kappa = 0.04J$, $d_1 = d_2 = 0$ (dissipative in solid magenta) and $d_1 = 0.04J$, $d_2 = 0$ (driven-dissipative in dashed green). Panels (c), (f), and (i) are the population dynamics for the left and right cavities for parameter specifications as in panels (b), (e), and (h), respectively. The dotted gray vertical lines in panels (b), (e), and (h) mark the break time t_{break} when the localization starts getting destroyed.

we see that the dissipative setup destabilizes the already localized regime by photon leakage. The case deep within the localized regime is presented in Fig. 11(g). In Fig. 11(h) we notice that, when the left cavity is coherently driven, the localized state persists even at long times. Furthermore, Fig. 11(i) demonstrates the balancing of drive and dissipation and attainment of a steady state with finite N_1 and $N_2 \approx 0$.

1. Optimum drive for stable localization

Figure 12 depicts the temporal stability of localization with varying d_1 when the system resides deep in the self-trapped regime. It is evident from Figs. 12(a) and 12(b) that there exists an optimum range of d_1 that reinforces N_1 as to stabilize z over long times. Jt_{break} is plotted in Fig. 12(c) where the upper limit of the y axis can be taken much greater than 1400 as in the phase (ii) region t_{break} actually diverges; we set this limit just for representation. Here we have constructive and destructive roles of photon drive at the two boundaries of optimum range. At lower bound, drive wins over dissipation, whereas it spoils steady-state localization at the upper bound. Although the two-cavity case is a special case of the 1-D lattice (Fig. 7) in the main text, they reflect similar physics.

2. Validity of semiclassical treatment

Here we discuss the validity of our semiclassical treatment and explicitly show the dynamics in the three phases in Fig. 8.

Our semiclassical treatment fails when the photon population becomes very small. This situation arises when the drive is

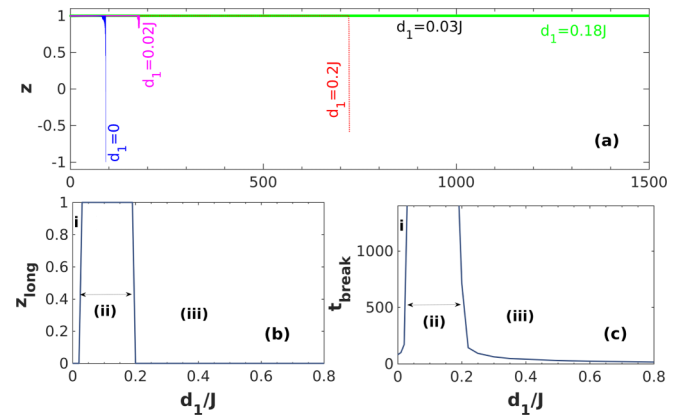


FIG. 12. Semiclassical behavior. (a) Temporal behavior of z for various d_1 values [$d_1 = 0, 0.02J, 0.03J, 0.18J, 0.2J$ presented as solid blue (dark), solid magenta (gray), dashed black, thick green (light gray), and dotted red (dark), respectively] when $g = 25J$ and $\gamma = \kappa = 0.04J$. (b) Long-time values of $z = z_{\text{long}}$ and (c) t_{break} for varying d_1 are plotted. These results in panels (b) and (c) show that semiclassical method predicts an abrupt change between no self-trapping and an indefinitely-long-lived trapped state. Here (i)–(iii) are the ranges of d_1 corresponding to the three phases already presented in Fig. 8.

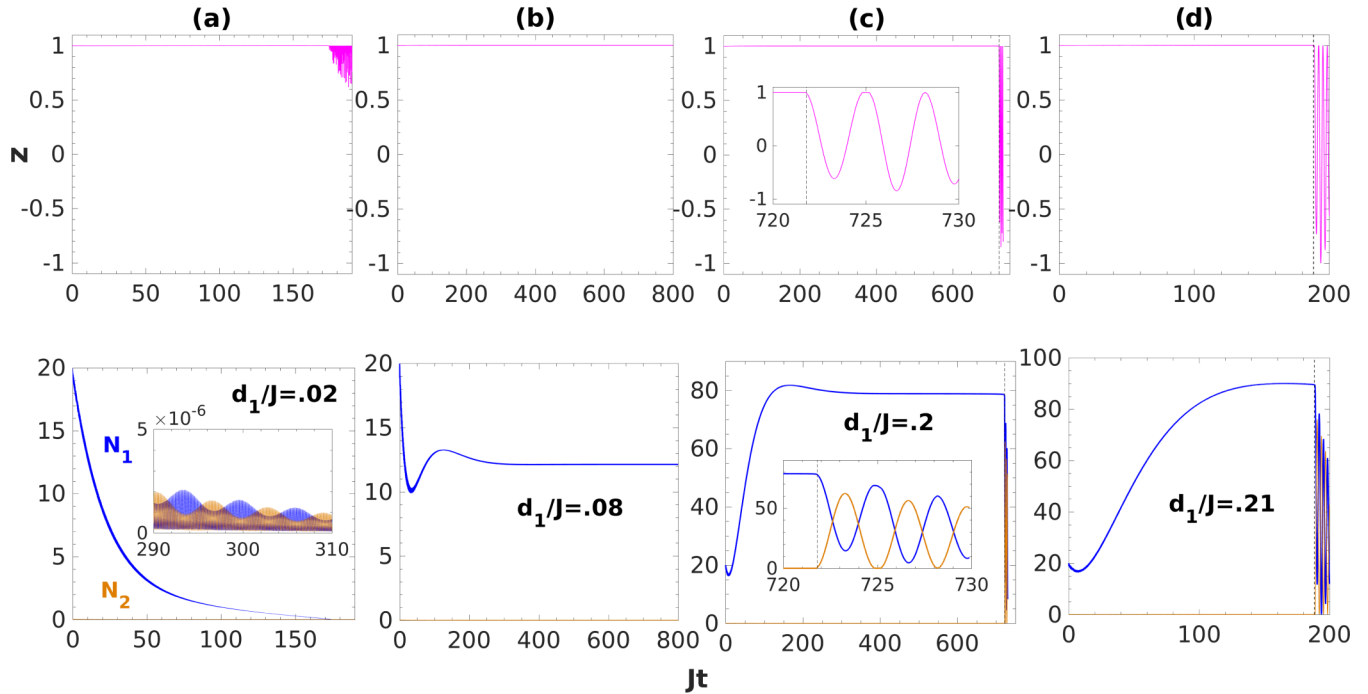


FIG. 13. Semiclassical results for various drives when $g_1 = g_2 = 25J$, $\kappa = \gamma = 0.04J$, and $d_2 = 0$. The plots are presented column-wise: Column (a) is the under-driven case, column (b) is indefinite self-trapping, columns (c) and (d) are the over-driven delocalized cases. Blue (dark) and orange (gray) solid lines in the lower panels present the first and second cavity populations, respectively. Vertical dashed lines mark the break time, where the localization is just destroyed.

unable to counter the dissipation and the photon population monotonically decays. This is the regime in phase (i) of Fig. 8. We plot such an instance in Fig. 13(a). Although the monotonic decay of population suggests no considerable population at long times, we cannot comment about the steady-state population, which is very small. The z oscillations here are due to the small-amplitude ripples in N_1 and N_2 [see inset of Fig. 13(a)] and the altering orders of N_1 and N_2 . These unphysical oscillations are attributed to the failure of the semiclassical approximation.

On the other hand, the scenario in phase (iii) is very different. In this over-driven regime we plot Fig. 13(c), where the first cavity population around the break time is considerably large and our semiclassical approach is valid. Beyond this point we see large population oscillation indicating delocalization. Here we took only a few oscillations that converged for various numerical precisions. At much longer times, the numerics does become very sensitive but we do not need to go to such long times since self-trapping has already been broken. However, comparing Fig. 13(b) (steady-state self-trapping located within the yellow region of Fig. 8) and Fig. 13(c) we note a drastic delocalization (which has physical significance) of an *already stabilized* population in Fig. 13(c). Therefore, d_1^{\max} separates two physically distinct phases of localization: (ii) indefinitely self-trapped and (iii) over-driven delocalized. In fact, our analytical phase boundary (magenta line) matches very well with the numerical phase boundary and it relies on the assumption $\langle a_2 \rangle \approx 0$. Any drive $d_1 > d_1^{\max}$ violates this assumption, making a localized steady state not possible. Note that, as we keep increasing the drive in phase (iii), unlike in phase (ii) the lifetime of localization

(limited by break time) becomes shorter [compare Figs. 13(c) and 13(d)].

3. Parameter-Space Description of Localization

Figure 14 depicts the parameter regime where localized steady state is accessible [(ii) yellow region]. Figure 14(b) demonstrates weak γ dependence of d_1^{\max} as a consequence of negligible photon loss via the spontaneous decay channel.

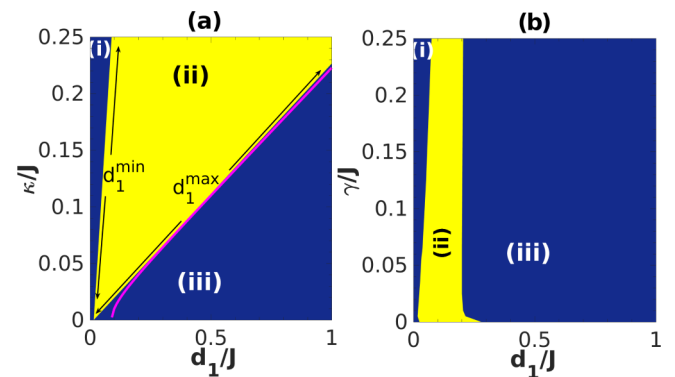


FIG. 14. Semiclassically obtained phase-space description of long-lived trapped state. (a) Description in d_1 - κ plane when $\gamma = 0.04J$. (b) Description in d_1 - γ plane when $\kappa = 0.04J$. In both figures, the cavity system is initialized to a state $\{20, 0, -1/2, -1/2\}$ and fixed coupling for both cases, $g_1 = g_2 = 25J$. The phases (i)–(iii) are the same as in Fig. 8.

- [1] G. J. Milburn, J. Corney, E. M. Wright, and D. F. Walls, *Phys. Rev. A* **55**, 4318 (1997).
- [2] A. Smerzi, S. Fantoni, S. Giovanazzi, and S. R. Shenoy, *Phys. Rev. Lett.* **79**, 4950 (1997).
- [3] S. Levy, E. Lahoud, I. Shomroni, and J. Steinhauer, *Nature (London)* **449**, 579 (2007).
- [4] M. Albiez, R. Gati, J. Fölling, S. Hunsmann, M. Cristiani, and M. K. Oberthaler, *Phys. Rev. Lett.* **95**, 010402 (2005).
- [5] H. Mabuchi and A. C. Doherty, *Science* **298**, 1372 (2002).
- [6] R. J. Schoelkopf and S. M. Girvin, *Nature (London)* **451**, 664 (2008).
- [7] A. A. Houck, H. E. Türeci, and J. Koch, *Nat. Phys.* **8**, 292 (2012).
- [8] I. A. Shelykh, D. D. Solnyshkov, G. Pavlovic, and G. Malpuech, *Phys. Rev. B* **78**, 041302(R) (2008).
- [9] M. Abbarchi, A. Amo, V. G. Sala, D. D. Solnyshkov, H. Flayac, L. Ferrier, I. Sagnes, E. Galopin, A. Lemaître, G. Malpuech, and J. Bloch, *Nat. Phys.* **9**, 275 (2013).
- [10] R. Coto, M. Orszag, and V. Eremeev, *Phys. Rev. A* **91**, 043841 (2015).
- [11] S. Schmidt, D. Gerace, A. A. Houck, G. Blatter, and H. E. Türeci, *Phys. Rev. B* **82**, 100507(R) (2010).
- [12] J. Raftery, D. Sadri, S. Schmidt, H. E. Türeci, and A. A. Houck, *Phys. Rev. X* **4**, 031043 (2014).
- [13] M. Greiner, O. Mandel, T. Esslinger, T. W. Hänsch, and I. Bloch, *Nature (London)* **415**, 39 (2002).
- [14] I. Bloch, J. Dalibard, and W. Zwerger, *Rev. Mod. Phys.* **80**, 885 (2008).
- [15] A. Dey and A. Vardi, *Phys. Rev. A* **95**, 033630 (2017).
- [16] H. J. Kimble, *Phys. Scr.* **T 76**, 127 (1998).
- [17] A. D. Greentree, C. Tahan, J. H. Cole, and L. C. L. Hollenberg, *Nat. Phys.* **2**, 856 (2006).
- [18] M. J. Hartmann, F. G. S. L. Brandão, and M. B. Plenio, *Nat. Phys.* **2**, 849 (2006).
- [19] D. Rossini and R. Fazio, *Phys. Rev. Lett.* **99**, 186401 (2007).
- [20] M. Aichhorn, M. Hohenadler, C. Tahan, and P. B. Littlewood, *Phys. Rev. Lett.* **100**, 216401 (2008).
- [21] O. T. Brown and M. J. Hartmann, *New J. Phys.* **20**, 055004 (2018).
- [22] J. J. Mendoza-Arenas, S. R. Clark, S. Felicetti, G. Romero, E. Solano, D. G. Angelakis, and D. Jaksch, *Phys. Rev. A* **93**, 023821 (2016).
- [23] M. Lieb and M. J. Hartmann, *New J. Phys.* **12**, 093031 (2010).
- [24] M. Fitzpatrick, N. M. Sundaresan, A. C. Y. Li, J. Koch, and A. A. Houck, *Phys. Rev. X* **7**, 011016 (2017).
- [25] S. Schmidt and J. Koch, *Ann. Phys. (Berlin, Ger.)* **525**, 395 (2013).
- [26] A. Wallraff, D. I. Schuster, A. Blais, L. Frunzio, R.-S. Huang, J. Majer, S. Kumar, S. M. Girvin, and R. J. Schoelkopf, *Nature (London)* **431**, 162 (2004).
- [27] N. M. Sundaresan, Y. Liu, D. Sadri, L. J. Szócs, D. L. Underwood, M. Malekakhlagh, H. E. Türeci, and A. A. Houck, *Phys. Rev. X* **5**, 021035 (2015).
- [28] K. W. Murch, U. Vool, D. Zhou, S. J. Weber, S. M. Girvin, and I. Siddiqi, *Phys. Rev. Lett.* **109**, 183602 (2012).
- [29] C. Aron, M. Kulkarni, and H. E. Türeci, *Phys. Rev. A* **90**, 062305 (2014).
- [30] C. Aron, M. Kulkarni, and H. E. Türeci, *Phys. Rev. X* **6**, 011032 (2016).
- [31] M. E. Kimchi-Schwartz, L. Martin, E. Flurin, C. Aron, M. Kulkarni, H. E. Türeci, and I. Siddiqi, *Phys. Rev. Lett.* **116**, 240503 (2016).
- [32] S. M. Hein, C. Aron, and H. E. Türeci, *Phys. Rev. A* **93**, 062331 (2016).
- [33] M. Kulkarni, S. M. Hein, E. Kapit, and C. Aron, *Phys. Rev. B* **97**, 064506 (2018).
- [34] K. Mølmer, Y. Castin, J. Dalibard, *J. Opt. Soc. Am. B* **10**, 524 (1993).
- [35] M. Boissonneault, J. M. Gambetta, and A. Blais, *Phys. Rev. A* **79**, 013819 (2009).
- [36] R. Ma, B. Saxberg, C. Owens, N. Leung, Y. Lu, J. Simon, and D. I. Schuster, *Nature (London)* **566**, 51 (2019).
- [37] A. Biella, F. Storme, J. Lebreuilly, D. Rossini, R. Fazio, I. Carusotto, and C. Ciuti, *Phys. Rev. A* **96**, 023839 (2017).
- [38] J. Lebreuilly, A. Biella, F. Storme, D. Rossini, R. Fazio, C. Ciuti, and I. Carusotto, *Phys. Rev. A* **96**, 033828 (2017).
- [39] A. J. Kollár, M. Fitzpatrick, and A. A. Houck, *Nature (London)* **571**, 45 (2019).